Available online at www.sciencedirect.com
ScienceDirect
Acta Materialia 56 (2008) 4369–4377
Acta MATERIALIA
www.elsevier.com/locate/actamat

Creep- and coarsening properties of Al–0.06 at.% Sc–0.06 at.% Ti at 300–450 °C

Marsha E. van Dalen [a,*], David N. Seidman [a,b], David C. Dunand [a]

[a] Department of Materials Science and Engineering, Northwestern University, 2220 Campus Dr., Evanston, IL 60208-3108, USA
[b] Northwestern University Center for Atom-Probe Tomography (NUCAPT), Northwestern University, 2220 Campus Dr., Evanston, IL 60208-3108, USA

Received 9 March 2008; received in revised form 1 May 2008; accepted 1 May 2008
Available online 2 June 2008

Abstract

Upon aging at 300–450 °C, nanosize, coherent $Al_3(Sc_{1-x}Ti_x)$ precipitates are formed in pure aluminum micro-alloyed with 0.06 at.% Sc and 0.06 at.% Ti. The outstanding coarsening resistance of these precipitates at these elevated temperatures (61–77% of the melting temperature of aluminum) is explained by the significantly smaller diffusivity of Ti in Al when compared to that of Sc in Al. Furthermore, this coarse-grained alloy exhibits good compressive creep resistance for a castable, heat-treatable aluminum alloy: the creep threshold stress varies from 17 MPa at 300 °C to 7 MPa at 425 °C, as expected if the climb bypass by dislocations of the mismatching precipitates is hindered by their elastic stress fields.

Keywords: Aluminum alloys; Nanostructure; Precipitation; Creep; Titanium

1. Introduction

Micro-alloying additions of scandium to aluminum (below the maximum solubility of 0.23 at.% Sc at the eutectic temperature) result, upon aging, in the formation of fine, coherent Al_3Sc precipitates with the $L1_2$ structure, which remain coarsening-resistant up to temperatures of ~300 °C [1–8]. When cast to produce coarse grains and aged to form fine Al_3Sc precipitates, binary Al–Sc alloys exhibit good creep resistance as a result of precipitation strengthening, up to about 300 °C [9,10]. Above 300 °C, however, rapid coarsening of the Al_3Sc precipitates leads to a loss in creep resistance. The addition of slower-diffusing elements, which are soluble in Al_3Sc, has the potential to increase the coarsening resistance of Al_3Sc precipitates and thus improve creep resistance of the alloy, in particular at temperatures beyond 300 °C.

Titanium is a promising candidate as a ternary alloying element to Al–Sc alloys, since it has the highest solid-solubility in aluminum of all trialuminide-forming elements [1], as well as a high solubility in Al_3Sc (up to half of the Sc atoms can be replaced [11]), leading to a reduction in the lattice parameter of the $Al_3(Sc_{1-x}Ti_x)$ phase [11]. Additionally, the tracer diffusivity of Ti in Al is significantly smaller than that of Sc in Al (by a factor of ca. 3×10^{-6} at 300 °C and 4×10^{-5} at 400 °C, respectively [1,12,13]), which may further reduce the precipitate coarsening kinetics and provide creep resistance at temperatures in excess of 300 °C [14]. A similar improvement in the coarsening resistance is obtained with the addition of Zr to Al–Sc alloys [15] and Re to Ni-based superalloys [16]. Indeed, in an electrical resistivity study, it was found that the addition of 0.06–0.17 at.% Ti to the hypereutectic Al–0.36 at.% Sc alloy stabilizes the precipitate structure at 300 °C [17]. In a recent study on a dilute, hypoeutectic Al–0.06Sc–0.06Ti (at.%) alloy, we demonstrated that Ti segregates at the α-Al/β-$Al_3(Sc_{1-x}Ti_x)$ heterophase interface and that the precipitates are remarkably coarsening-resistant at 300 °C [14], with time exponents smaller than predicted by a mean-field coarsening model for a ternary alloy [18].

* Corresponding author. Tel.: +1 847 712 8765.
E-mail address: vandalen@u.northwestern.edu (M.E. van Dalen).

1359-6454/$34.00 © 2008 Acta Materialia Inc. Published by Elsevier Ltd. All rights reserved.
doi:10.1016/j.actamat.2008.05.002

The Al–Sc–Zr system has been studied extensively and shows many parallels to the Al–Sc–Ti system [1]. Zirconium partitions to the Al_3Sc precipitates, forming coarsening-resistant $Al_3(Sc_{1-x}Zr_x)$ precipitates [15,19], which retain their $L1_2$ structure with up to half the Sc atoms being replaced by Zr atoms [11,20]. In Al–Sc–Zr alloys, however, the Zr concentrations in the precipitates are found to be smaller than this maximum value of $x = 0.5$ [15,21] as a result of the small diffusivity of Zr in Al [13]. Several experimental studies show that Zr segregates at the α-Al/β-Al_3Sc heterophase interface forming a spherical Zr-rich shell surrounding the Al_3Sc precipitates [19,21–25]. Lattice kinetic Monte Carlo simulations demonstrate that the formation of this shell is due to a disparity in diffusivities between Zr and Sc [26]. Differences between the Al–Sc–Zr and Al–Sc–Ti systems include a much larger diffusivity of Zr in Al (by a factor of ~20 at 300 °C [12]) and a much smaller maximum solid-solubility of Zr in Al (by a factor of ~10), as compared with those of Ti in Al [27].

Prior studies on coarse-grained, dilute Al–Sc-based alloys – binary Al–Sc alloys [6,9,10] as well as ternary Al–Mg–Sc [28,29], Al–Sc–Zr [15,23,30], Al–Sc–Ti [14] and Al–Sc–RE alloys [31–33] (RE = rare earth element) – demonstrate that these alloys are coarsening and creep resistant up to 300 °C. With Ti additions, the precipitates are expected to retain their coarsening resistance at temperatures significantly greater than 300 °C [14], thus imparting creep resistance to the alloy at higher temperatures. The present article demonstrates that this hypothesis is correct and reports on the microstructure and creep properties of a dilute ternary Al–Sc–Ti alloy at temperatures in the range of 300–450 °C, corresponding to homologous temperatures $T/T_{m,Al} = 0.61$–0.77 (where $T_{m,Al} = 933$ K is the melting temperature of aluminum).

2. Experimental procedures

The same alloy as used in a previous creep study at 300 °C [14] was utilized, with the composition Al–0.06Sc–0.06Ti (at.%), corresponding to Al–0.10 wt.% Sc–0.10 wt.% Ti (all compositions are in at.% in the remainder of this article unless otherwise noted). This dilute composition was chosen so that the alloy was in the α-Al phase field during homogenization. The alloy was produced by diluting small quantities of Al–1.2% Sc (Ashurst) and Al–2.26% Ti (Alcoa) master alloys with 99.99% pure Al in an alumina crucible in a resistively heated furnace at 750 °C in air. After thorough stirring, the melt was cast into a graphite mold resting on a large copper platen. Homogenization was performed at 640 °C for 72 h in air and terminated by water-quenching to room temperature, resulting in large grain sizes on the order of ~1 mm. The composition of the homogenized alloy was verified by Luvak Inc. (Bolyston, MA) to be 0.060 ± 0.003% Sc and 0.059 ± 0.003% Ti with very low concentrations of Fe and Si impurities (0.0022 ± 0.0003 and 0.0038 ± 0.0005%, respectively). Aging treatments were performed in air on creep samples machined into cylinders 8 mm in diameter and 16 mm in length. The samples to be creep-tested at 300–400 °C were subjected to a double-aging treatment consisting of 24 h at 300 °C followed by 120 h at 400 °C. Samples to be crept at the highest temperatures of 425–450 °C were triple-aged as follows: 24 h at 300 °C, 240 h at 400 °C and 48 h at 450 °C.

To ensure a uniform temperature during creep testing, the samples were soaked at the testing temperature for 2 h prior to loading. Creep tests were performed in a nickel-based superalloy compression cage and the sample ends were lubricated with boron nitride to reduce friction between the cage and the sample. The displacement was measured with a linear variable differential transducer connected to an extensometer. Sufficient time was allowed to reach a minimum strain-rate for each successively higher load applied to the sample. The creep experiments were terminated when a sample achieved a total strain of 10%. No sample was crept longer than 10 days to ensure that the precipitates did not coarsen significantly during the test. Vickers microhardness measurements were performed at room temperature using a 200 g load for 10 s on aged samples that were mounted in acrylic and ground to a 1 μm surface finish. Ten measurements were performed on each sample.

Sample blanks for local-electrode atom-probe (LEAP™) tomography were produced by mechanically grinding material to a square cross-section of ca. 300×300 μm^2. An atomically sharp tip was then created by electropolishing, starting with a solution of 10 vol.% perchloric acid in acetic acid and finishing with a solution of 2 vol.% perchloric acid in butoxyethanol. LEAP tomography was performed using a LEAP Si instrument (Imago Scientific Instruments, Madison, WI) [34,35] operating in voltage pulsing mode at a specimen temperature of 30 K, at a pulse repetition rate of 200 kHz and with a 20% pulse fraction (pulse voltage divided by steady-state DC voltage). Proximity histogram plots (proxigrams [36]) were calculated employing the APEX [37] or IVAS (Imago Scientific Inst.) software programs, using an isoconcentration surface of 9 at.% Sc (corresponding to the inflection point in the concentration vs. distance curve). The average precipitate composition was determined by counting the number of atoms in the precipitates with the interface set at the inflection point on the Sc concentration profile.

Transmission electron microscopy (TEM) was used to determine the precipitate radii and was performed using a Hitachi 8100 at an accelerating voltage of 200 kV. Foils were mechanically ground to a thickness of 200 μm and subsequently electropolished in a solution of 5 vol.% perchloric acid in methanol at −25 °C.

3. Experimental results

3.1. Microstructure and composition

The addition of Ti results in precipitates that are coarsening-resistant and remain nanosize and spheroidal upon

double aging (Fig. 1) and triple aging. The samples are aged initially at 300 °C for 24 h to nucleate and initiate the growth of the precipitates at a temperature with a high solute supersaturation, thereby forming a high number density of precipitates. Subsequently, the samples are aged at higher temperatures (400 °C for 120 h for the doubly aged sample and an additional 120 h at 400 °C and 48 h at 450 °C for the triply aged sample) to grow and coarsen the precipitates at a temperature at least as high as the creep temperature. The double-aged samples, with a final aging treatment at 400 °C, exhibit an average precipitate radius of $\langle R\rangle = 8.3 \pm 2.9$ nm. These precipitates are coherent with the α-Al matrix, as illustrated by the Ashby–Brown strain-field contrast visible in Fig. 2. For the triple-aging treatment, $\langle R\rangle$ increases modestly to 10.0 ± 0.8 nm, despite a significantly higher final aging temperature of 450 °C (the root-mean-square Ti diffusion distance quadruples from 39 to 162 nm from the double to the triple-aging treatment). In contrast, it was found previously that a single-aging treatment performed at or above 330 °C on the present alloy led to precipitates that were heterogeneously nucleated, resulting in a near total loss of strengthening [14].

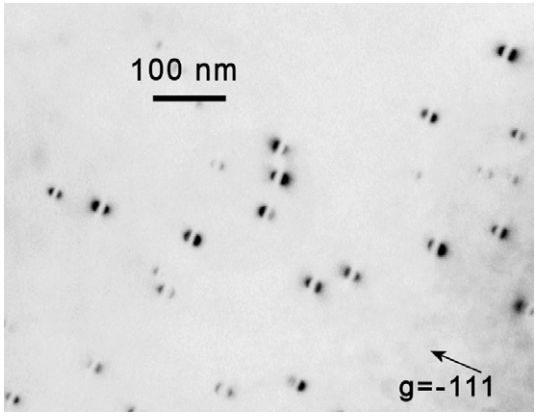

Fig. 2. Two-beam bright-field TEM image ([1 1 0] projection) after double aging (24 h at 300 °C and 120 h at 400 °C), showing $Al_3(Sc_{1-x}Ti_x)$ precipitates with Ashby–Brown strain-field contrast indicative of coherent precipitates.

The concentration of Ti within the $Al_3(Sc_{1-x}Ti_x)$ precipitates after double aging (24 h/300 °C and 120 h/400 °C) is $C^{\beta}_{Ti} = 2.8 \pm 0.1\%$ Ti, with confined (nonmonotonic) segregation of Ti near the α-Al/β-$Al_3(Sc_{1-x}Ti_x)$ matrix/precipitate heterophase interface (visible as a shell in Fig. 1), where a maximum concentration of 5.8% Ti is found (Fig. 3). This corresponds to a relative Gibbsian interfacial excess of Ti atoms compared to Al and Sc atoms at the α-Al/β-$Al_3(Sc_{1-x}Ti_x)$ interface of 3.9 atoms nm^{-3} (calculated using the same procedure as in Refs. [14,38]). The α-Al matrix concentration of Ti, after the double-aging treatment, is $C^{\alpha}_{Ti} = 0.033 \pm 0.005\%$, corresponding to about half its initial value (Fig. 4). By contrast, the Sc matrix

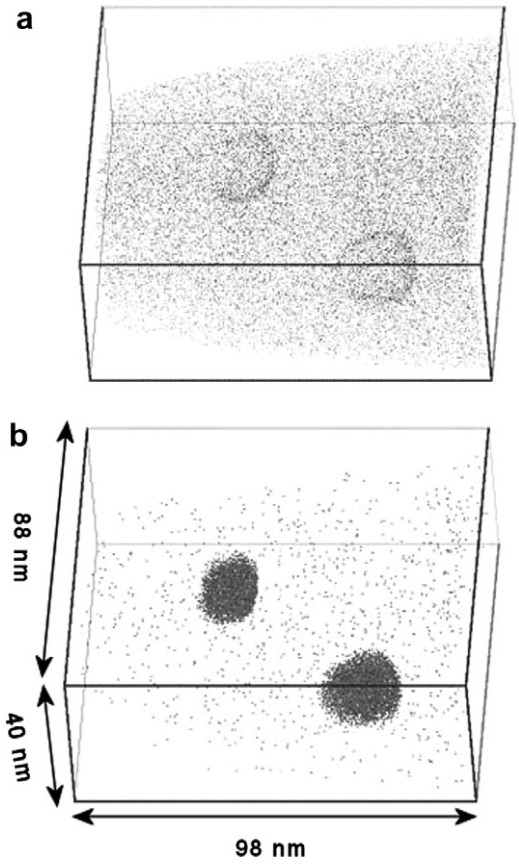

Fig. 1. Three-dimensional reconstruction of LEAP tomographic data displaying two $Al_3(Sc_{1-x}Ti_x)$ precipitates in the α-Al matrix after double aging (24 h at 300 °C and 120 h at 400 °C). The data set contains 7.7 million atoms. (a) Only Ti atoms are displayed, indicating segregation of Ti at the heterophase interface. About half of the Ti atoms remain in the matrix ($C^{\alpha}_{Ti} = 0.033$ at.%). (b) Only Sc atoms are displayed, indicating strong partitioning of Sc to the precipitate phase with very few Sc atoms remaining in the α-Al matrix.

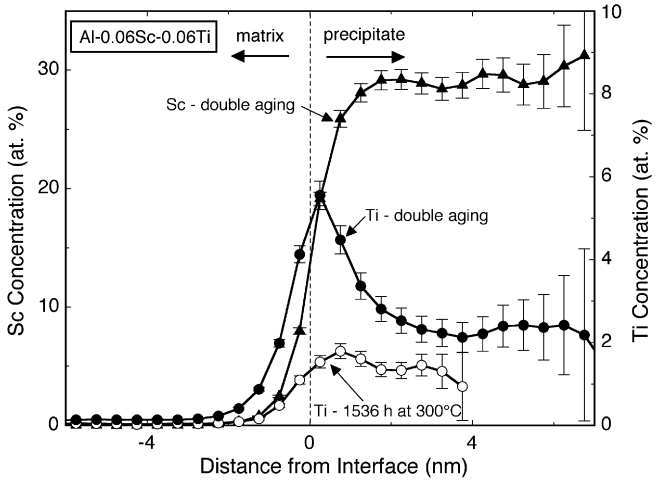

Fig. 3. LEAP tomographic proxigram of $Al_3(Sc_{1-x}Ti_x)$ precipitates after double aging (24 h at 300 °C and 120 h at 400 °C). The dashed line indicates the interface between the α-Al and $Al_3(Sc_{1-x}Ti_x)$ phases (based on an isoconcentration surface of 9 at.% Sc), clearly showing the segregation of Ti at the heterophase interface. Also shown is a proxigram for the same alloy after single aging (1536 h at 300 °C) from Ref. [14], with a smaller root-mean-square Ti diffusion distance, ($\sqrt{4Dt}$).

concentration is $C_{Sc}^{\alpha} = 0.0037 \pm 0.0005\%$, indicating that most of the Sc has partitioned to the precipitate phase.

3.2. Mechanical properties at ambient and elevated temperatures

The alloy microhardness at ambient temperature, measured previously for single aging at 300 °C [14] and measured here for the double and triple-aging treatments, is plotted in Fig. 5 as a function of the total Ti diffusion distance: $\sum(4D(T)\cdot t)^{1/2}$, where $D(T)$ is the tracer diffusivity of Ti in Al at the aging temperature T ($D(T) = 2.74 \times 10^{-25}$ and 8.86×10^{-22} m^2 s^{-1} at 300 and 400 °C, respectively [12]), and t is the corresponding aging time. It is apparent from Fig. 5 that the decrease in microhardness from single aging at 300 °C for 1536 h to double aging at 300 and 400 °C is modest (about 20 MPa). The microhardness of the double-aged specimens remains constant after long-term creep at 300–400 °C, even after doubling the root-mean-square Ti diffusion distance.

Triple aging at 300, 400 and 450 °C leads to a further small decrease in hardness (25 MPa) as compared to the double-aging treatment, and the specimen crept subsequently at 425 °C retains its microhardness within experimental error, which is indicative of negligible precipitate coarsening at 425 °C (homologous temperature of 0.75). Creep at 450 °C for 10 days leads, however, to a near complete loss of hardening after the creep test (the microhardness in the as-quenched state before precipitation is 210 MPa). This is indicative of significant coarsening during the creep experiments at 450 °C, and hence the results of these creep experiments are not reported.

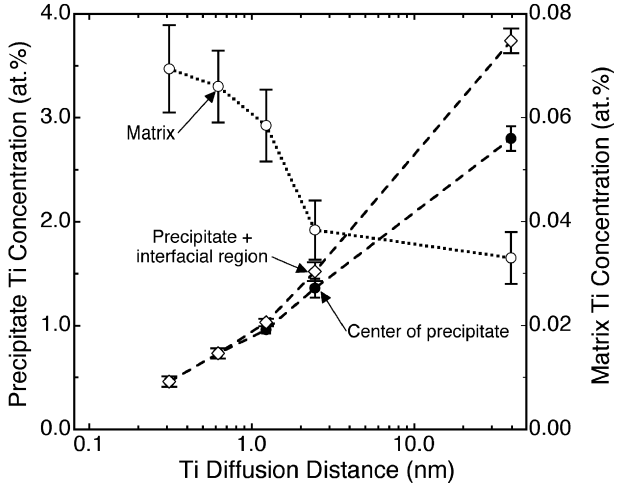

Fig. 4. Ti concentration in the $Al_3(Sc_{1-x}Ti_x)$ precipitates and the α-Al matrix as measured by LEAP tomography vs. root-mean-square Ti diffusion distance ($\sqrt{4Dt}$). The data points with diffusion distances less than 3 nm are for samples single-aged at 300 °C for 24–1536 h (1–64 days) from Ref. [14]. The double-aging treatment (24 h at 300 °C and 120 h at 400 °C) used for the present creep samples gives a significantly larger diffusion distance.

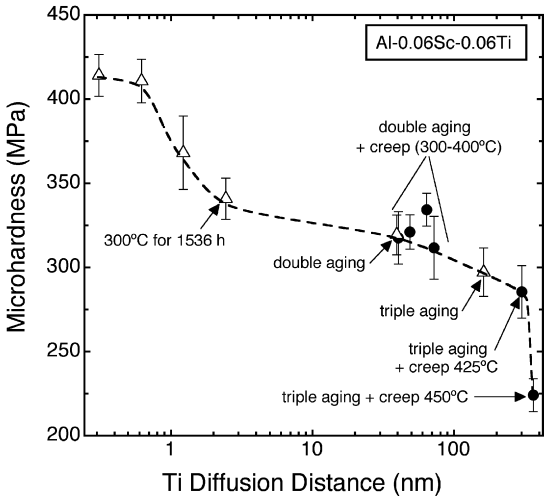

Fig. 5. Vickers microhardness vs. root-mean-square Ti diffusion distance ($\sqrt{4Dt}$). Open symbols represent microhardness values for samples before creep and after aging (either single aging at 300 °C [14], double aging at 300 and 400 °C, or triple aging at 300, 400 and 450 °C). Solid symbols represent microhardness values of aged samples after creep testing.

Values of $\langle R\rangle$ after single aging at 300 °C for 24 h (peak aging) and 1536 h as well as after the double- and triple-aging treatments, are plotted in Fig. 6 as a function of the yield stress increment, calculated as one third of the microhardness increment (microhardness value subtracted from the as-quenched microhardness) [39]. Also displayed in Fig. 6 is the theoretical Orowan stress increment, $\Delta\sigma_{Or}$, as given by Ref. [40]

$$\Delta\sigma_{Or} = M\frac{0.4Gb}{\pi\lambda}\frac{\ln(2\overline{R}/b)}{\sqrt{1-v}} \quad (1)$$

where $M = 3.06$ is the orientation factor for aluminum [41], $G = 25.4$ GPa [42] is its shear modulus, $v = 0.345$ is its

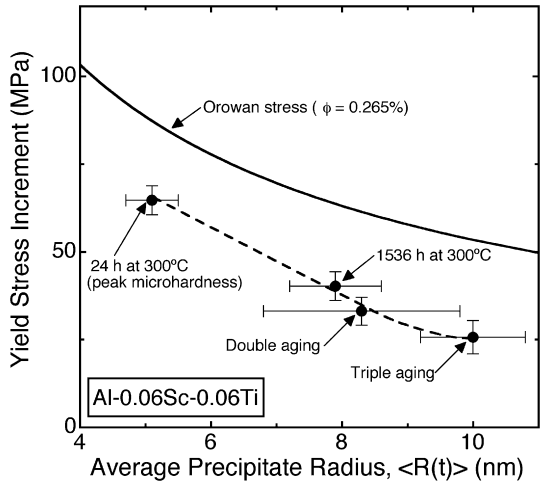

Fig. 6. Yield stress increment (as calculated from Vickers microhardness) vs. average $Al_3(Sc_{1-x}Ti_x)$ precipitate radius (as determined by TEM) for single aging at 300 °C [14], double aging (300 and 400 °C), or triple aging (300, 400 and 450 °C).

Poisson's ratio, $b = 0.286$ nm [42] is the magnitude of its Burgers vector, λ is the inter-precipitate spacing and $\overline{R} = \pi/4\langle R\rangle$ is the mean planar radius [43]. Although the predicted Orowan stress increment is somewhat larger than the measured yield stress increment, the general trend of decreasing values with increasing $\langle R\rangle$ indicates that Orowan strengthening is the operating mechanism at these radii at room temperature, in agreement with previous studies on Al–Sc [10], Al–Sc–Zr [30] and Al–0.06Sc–0.005RE (RE = Yb or Gd) [32] alloys.

Fig. 7 presents the minimum creep strain-rate, $\dot{\varepsilon}$, as a function of the applied compressive stress, σ, for double-aged samples tested in the range of 300–400 °C and for a triple-aged sample tested at 425 °C. The minimum creep rate is determined by plotting strain-rate vs. time to ascertain that a minimum value is truly achieved. The minimum rate can be fitted to a power-law equation

$$\dot{\varepsilon} = A_{\mathrm{ap}}\sigma^{n_{\mathrm{ap}}}\exp\left(\frac{-Q_{\mathrm{ap}}}{R_{\mathrm{g}}T}\right) \tag{2}$$

where A_{ap} is a constant, n_{ap} is the apparent stress exponent, Q_{ap} is the apparent activation energy and R_{g} is the universal gas constant. The high value of the apparent stress exponent ($n_{\mathrm{ap}} = 18$–35, Fig. 7) is indicative of a threshold stress, σ_{th}, below which creep is not measurable. The data can then be fitted to a modified power-law equation

$$\dot{\varepsilon} = A(\sigma - \sigma_{\mathrm{th}})^{n}\exp\left(-\frac{Q}{R_{\mathrm{g}}T}\right) \tag{3}$$

where A, n and Q are, respectively, the Dorn constant, the stress exponent and activation energy for diffusion in pure Al [42]. Values for the threshold stresses, as determined by plotting $\dot{\varepsilon}^{1/n}$ vs. σ (with $n = 4.4$ [42]), are indicated in Fig. 7.

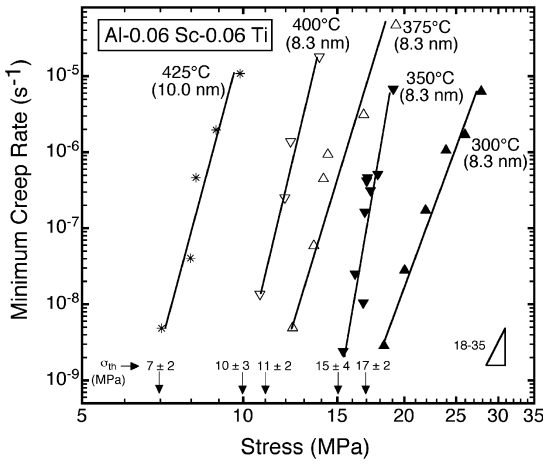

Fig. 7. Minimum creep strain-rate vs. applied compressive stress for double-aged (300 and 400 °C) samples creep-tested at 300–400 °C and a triple-aged (300, 400 and 450 °C) sample creep-tested at 425 °C. Testing temperature, average precipitate radius, and threshold stress are marked next to data.

4. Discussion

4.1. Microstructure and composition

The low coarsening rates of the $Al_3(Sc_{1-x}Ti_x)$ precipitates (Figs. 5 and 6) at temperatures up to 450 °C are linked to the small diffusivity of Ti in the α-Al matrix (2.2×10^{-20} m^2 s^{-1} as compared to 1.7×10^{-16} m^2 s^{-1} for Sc in Al at 450 °C) [12]. It is also observed that the Ti remains localized at the α-Al/β-$Al_3(Sc_{1-x}Ti_x)$ interface. This can be attributed to the fact that diffusion is generally slower in the $L1_2$ precipitates, as compared to diffusion in the disordered solid-solution FCC matrix, due to a smaller value of the correlation factor for diffusion in an ordered structure ($L1_2$).

With the creep temperatures approaching the aging temperatures, coarsening of the precipitates during the creep experiments must be considered. In fact, it was observed in an Al–Mg–Li–Zr–Sc–Zn alloy that the Al_3(Sc,Zr) precipitates coarsen faster under stress [44]. $\langle R\rangle$ was found in that study to be proportional to $t^{1/3}$ but the coarsening rate constant was higher, when compared with specimens at the same temperature aged in the unstressed state. Faster coarsening during creep was also found in a magnesium-based alloy [45].

In the present study, the Al–Sc–Ti alloy retains its hardness after the creep experiments up to temperatures of 425 °C (Fig. 5), indicating that coarsening was negligible and the creep tests valid, for the testing times employed (<10 days). The exception is the sample crept at 450 °C, which exhibited a large decrease in microhardness, which is indicative of an increase in $\langle R\rangle$ and a loss of coherency.

The change in precipitate volume fraction, ϕ, with creep temperature must also be considered. For the samples undergoing the double-aging treatment $\phi = 0.27 \pm 0.02$ vol.%. The value of ϕ is directly calculated by subtracting the solute content in the matrix after aging from the overall solute content in the as-quenched state (both found by LEAP tomographic measurements), assuming that the amount of solute no longer in the matrix resides in the precipitate phase with the stoichiometric trialuminide composition. Since the solubility of Sc in the α-Al matrix increases with increasing temperature, C^{α}_{Sc} and hence ϕ could change during creep. LEAP tomographic measurements show, however, that only a small increase in C^{α}_{Sc} occurs for aging at higher temperatures: $C^{\alpha}_{\mathrm{Sc}} = 0.0037 \pm 0.0005\%$ after aging at 400 °C for 120 h, while $C^{\alpha}_{Sc} = 0.0016 \pm 0.0012\%$ after extended (1536 h) aging at 300 °C. This corresponds to a decrease of ϕ of only 0.01 vol.%, upon aging at 400 °C.

An additional factor affecting the value of ϕ is that the Ti concentration in the precipitates increases slowly up to the double-aging treatment. As shown in Fig. 4, beyond 1536 h of aging, C^{α}_{Ti} decreases slowly ($0.04 \pm 0.006\%$ after 1536 h of aging at 300 °C [14] compared with $0.033 \pm 0.005\%$ for the double-aging treatment). The equilibrium solubility of Ti, however, is not anticipated to be

much smaller than this value, since Murray's calculation of the ternary phase diagram [46] yields 0.01% at 300 °C and 0.047% at 400 °C for the solubility of Ti in the α-Al matrix. Ab initio calculations by Liu and Asta [47,48] of the binary Al–Ti system yielded a larger Ti solubility of 0.11% for metastable Al_3Ti ($L1_2$) at 300 °C. This discrepancy may be due to the presence of Sc reducing the Ti solubility in the α-Al matrix. These solubility values indicate that the volume fraction of precipitates should not increase significantly during creep due to Ti additions to the precipitates, since the observed Ti concentrations in the α-Al matrix are less than the calculated solubility values.

4.2. Effect of temperature on creep properties

The creep rate is strongly sensitive to temperature (Fig. 7). To eliminate the effect of the threshold stress, the strain-rate can be considered at constant effective applied stress ($\sigma - \sigma_{th}$), defined as the difference between the applied stress and the threshold stress. By plotting $\dot{\varepsilon}$ vs. T^{-1} at constant effective applied stress on an Arrhenius plot according to Eq. (3), the activation energy for creep, Q, is found to be $Q = 130 \pm 20$ kJ mol^{-1}. This value is, within experimental error, equal to the activation energy for Al diffusion in the α-Al matrix (124 kJ mol^{-1} [49]). This suggests that climb of matrix dislocations over precipitates is the operating mechanism, which is controlled by flow of matrix vacancies biased by the effective stress, as previously described for dispersion- [50] and precipitation-strengthened alloys [51].

Other mechanisms, such as precipitate shearing or bypass by the Orowan looping mechanism, can be excluded since the experimental threshold stresses are much smaller than the ambient temperature yield stress determined from hardness measurements [14]. The activation energy we find is similar to those determined for an Al–0.12%Sc alloy (225–300 °C) [10], and for a direct chill cast Al–Cu–Mn–Cr–Zr–Fe alloy (250–500 °C) [52], where it was also concluded that dislocation climb is the operating mechanism.

The threshold stress, σ_{th}, decreases with increasing temperature, as shown in Fig. 7, and the rate of decrease is faster than that of the shear modulus, G (Fig. 8). Previous studies also found a temperature dependence of σ_{th}/G [53,54], which can be expressed as

$$\frac{\sigma_{th}}{G} = B_o \exp\left(\frac{Q_o}{R_g T}\right) \quad (4)$$

where B_o is a constant and Q_o is the activation energy associated with a dislocation overcoming an obstacle [52], although some authors remain uncertain as to its significance [55,56]. In Eq. (4), the temperature-dependent shear modulus for aluminum is $G = G_o[(1 - (T - 300)/2)/T_m]$, where $G_o = 25.4$ GPa and $T_m = 933$ K [42]. The activation energy $Q_o = 20 \pm 5$ kJ mol^{-1} is determined by plotting $\ln(\sigma_{th}/G)$ vs. $1/T$, according to Eq. (4). The value of σ_{th} at 425 °C was not used in this calculation, because it corresponds to a different pre-aging treatment and the alloy has a different $\langle R \rangle$. This small value of Q_o is most likely an effective activation energy for a complex physical process or processes for dislocation bypass of precipitates.

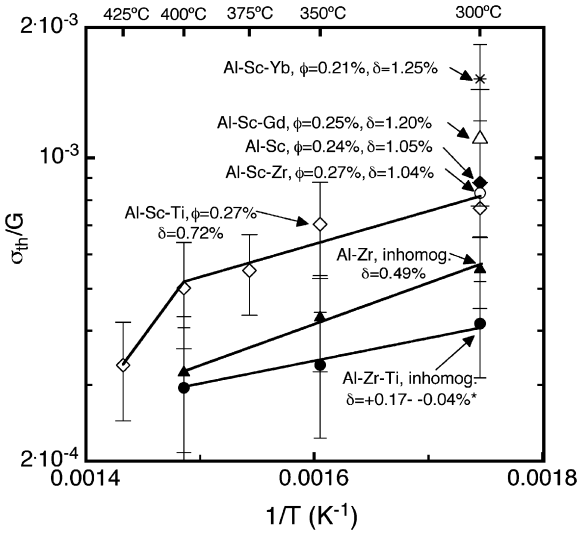

Fig. 8. Arrhenius plot of threshold stress σ_{th} (normalized by the temperature-dependent shear modulus G) vs. inverse creep temperature for Al–0.06Sc–0.06Ti. Literature data for other coarse-grained, cast, precipitation-strengthened alloys are also shown: Al–0.06Sc–0.005Yb [32], Al–0.06Sc–0.005Gd [32], Al–0.06Sc–0.005Zr [30], Al–0.06Sc [10], Al–0.1Zr [69,70] and Al–0.1Zr–0.1Ti [69,70] (the latter two alloys have inhomogeneous precipitate distributions). The lattice parameter mismatch values between precipitates and matrix are listed for 300 °C.

To explain the decrease in threshold stress with increasing temperature, previous studies considered the temperature sensitivity of mechanisms such as detachment of dislocations from particles [55,57,58], impurities at the interface [59] or interfacial dislocations [60]. These mechanisms apply to the interaction of dislocations with incoherent precipitates, and are therefore not relevant to the coherent precipitates in the present Al–Sc–Ti alloy. A decrease in the threshold stress in alloys with coherent precipitates [61] has also been discussed for the case where precipitates are sheared, which is again not applicable to the present Al–Sc–Ti alloy. Additionally, it was suggested that the decrease in threshold stress with increasing temperature can be attributed partially to the decrease in the value of precipitate volume fraction [54]. In the Al–Sc–Ti system, however, there is only a small change in volume fraction with increasing temperature, as discussed previously.

The mechanism controlling creep in the present Al–Sc–Ti alloy is expected to be dislocation bypass of precipitates according to the general climb model [62–65], which predicts a small threshold stress (about 0.06% of the Orowan stress [65]) independent of precipitate radius. If the precipitates exhibit a lattice parameter mismatch with the matrix, as in the present case, elastic interactions with the climbing dislocations make the bypass more difficult, resulting in threshold stress values that increase rapidly with increasing precipitate radius, as modeled in Refs. [51,66] and observed in numerous Al–Sc-based alloys [10,29,30]. A higher creep

temperature is expected to reduce the threshold stress by enhancing the kinetics of climb bypass as the vacancy diffusivity increases exponentially with temperature. An additional mechanism is the reduction in lattice parameter mismatch between precipitates and matrix with increasing temperature due to the differences in the coefficients of thermal expansions between the two phases. This effect is, however, small in the present system: the unconstrained lattice parameter mismatch decreases from 0.72% at 300 °C to 0.70% at 425 °C, using the compositions of the Al–Sc–Ti system as determined by LEAP tomographic composition measurements and the thermal expansion coefficient for binary Al_3Sc [67].

4.3. Effect of lattice parameter mismatch on creep properties

Plotted in Fig. 8 are threshold stresses for aluminum alloys with coherent, nanosize precipitates similar to those in the present alloy, but with a range of lattice parameter mismatches between precipitates and the α-Al matrix. For the seven alloys shown, it is apparent that, with increasing mismatch, the threshold stress at 300 °C increases. For instance, a binary Al–0.06Sc alloy exhibits a larger threshold stress than the present Al–0.06Sc–0.06Ti alloy, as expected from its larger lattice parameter mismatch ($\delta = 1.05\%$ vs. $\delta = 0.72\%$ [11]), despite near identical average precipitate radius and volume fractions ($\langle R\rangle = 8.5 \pm 0.5$ nm, $\phi = 0.24\%$ [10,67] for Al–Sc vs. $\langle R\rangle = 8.3 \pm 2.9$ nm, $\phi = 0.27\%$ for Al–Sc–Ti). Fig. 8 also demonstrates that the threshold stresses for Al–0.06Sc–0.005Yb (Al–Sc–Yb) and Al–0.06Sc–0.005Gd (Al–Sc–Gd) alloys [32] are significantly greater than for the present Al–Sc–Ti alloy. The lattice parameter mismatches for these alloys are $\delta = 1.25\%$ and 1.20%, respectively, much greater than $\delta = 0.72\%$ for the present Al–Sc–Ti alloy. The Al–Sc [6] and ternary Al–Sc–RE alloys [68], however, coarsen rapidly above 300 °C, even upon double aging, and thus lose their creep resistance above that temperature.

Comparisons at higher temperatures can be made with several alloys with more coarsening-resistant precipitates. A recent study of Al–0.1Zr (Al–Zr) and Al–0.1Zr–0.1Ti (Al–Zr–Ti) alloys [69,70] found threshold stresses smaller than for the present Al–Sc–Ti alloy (Fig. 8). This is in agreement with the smaller lattice parameter mismatches exhibited at 300 °C by these alloys: 0.49% for Al–Zr and ranging from +0.17% to −0.04% for Al–Zr–Ti (these values are estimations, since the exact composition of the precipitates was not measured, and their coefficients of thermal expansion were assumed equal to that of Al_3Sc). Also, these Al–Zr and Al–Zr–Ti alloys exhibit precipitate-free and precipitate-rich zones as a result of their peritectic solidification behavior, so their precipitate volume fraction is not well defined [1,71]. Finally, a recent study on an Al–0.07Sc–0.02Zr (Al–Sc–Zr) alloy demonstrates a larger normalized threshold stress than the Al–Sc–Ti alloy, as expected from its larger lattice parameter mismatch ($\delta = 1.04\%$ at 300 °C) with $\langle R\rangle = 8.7$ nm [30]. In summary,

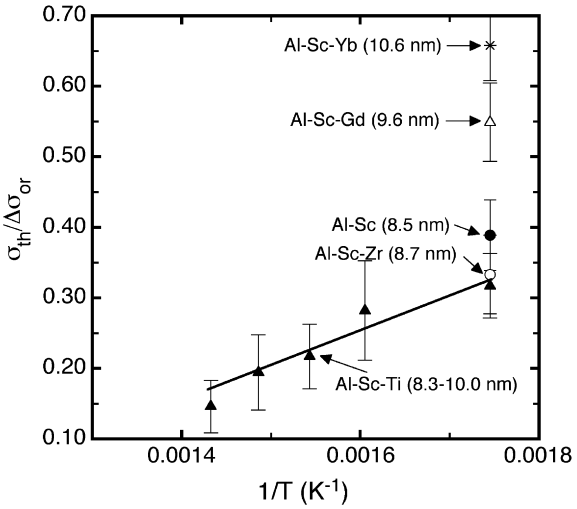

Fig. 9. Threshold stress σ_{th} (normalized by the calculated Orowan stress $\Delta\sigma_{Or}$) vs. inverse creep temperature. All data points have similar average radii (given in parentheses), which permits a direct comparison at 300 °C between the present Al–0.06Sc–0.06Ti alloy and Al–0.06Sc [10], Al–0.07Sc–0.02Zr [30], Al–0.06Sc–0.005Yb, and Al–0.06Sc–0.005Gd [32].

all of the above-mentioned alloys appear to validate the model based on a general climb bypass mechanism affected by precipitate lattice strains, predicting that the threshold stress scales with the lattice parameter mismatch between matrix and precipitates [51].

Fig. 9 displays a plot of the threshold stress, normalized by the calculated Orowan stress (Eq. (1)), as a function of the inverse temperature. This normalization procedure allows for comparison among samples with different precipitate volume fractions and radii. For the present Al–Sc–Ti alloy, the volume fraction varies little with creep temperature, and the average precipitate radii are all within a narrow range of 8.3–10 nm. Thus, the steep decrease with temperature of the normalized threshold stress (Fig. 9) reflects the decrease in the absolute magnitude of the threshold stress displayed in Fig. 7. For the Al–Sc, Al–Sc–Zr, Al–Sc–Yb and Al–Sc–Gd alloys (the same alloys plotted in Fig. 8), the threshold stresses were only measured at 300 °C. The alloys with the larger lattice parameter mismatches have higher normalized threshold stresses, confirming the trend observed in Fig. 8, while accounting for differences in volume fraction between the alloys.

5. Conclusions

Cast, coarse-grained aluminum with micro-alloying additions (0.06 at.%) of both Sc and Ti was subjected to multi-step aging treatments up to 450 °C to produce precipitates. The following findings are reached:

- Titanium is incorporated into the $Al_3(Sc_{1-x}Ti_x)$ precipitates ($L1_2$ structure), whose Ti content increases with increasing aging time and temperature, especially at the α-Al/β-$Al_3(Sc_{1-x}Ti_x)$ heterophase interface where Ti segregates.

- The $Al_3(Sc_{1-x}Ti_x)$ precipitates remain nanosize ($\langle R \rangle \leqslant 10$ nm) and coherent up to 450 °C for total root-mean-square Ti diffusion distances as large as 300 nm. This exceptional coarsening resistance is attributed to the significantly smaller diffusivity of Ti in Al as compared to that of Sc in Al.
- The precipitates hinder the motion of matrix dislocations, thus providing creep resistance to the Al–Sc–Ti alloy in the temperature range of 300–425 °C as demonstrated by sizeable creep threshold stresses (decreasing from 17 to 7 MPa over this temperature range).
- The small reduction of lattice parameter mismatch between precipitates and matrix due to the substitution of Sc by Ti results in a slight reduction of the normalized threshold stresses as compared to binary Al–Sc alloys with the same mean precipitate radii. Titanium-free precipitates in Al–Sc alloys coarsen rapidly above 300 °C, thereby rendering the alloys unsuitable for creep applications. This is unlike the present ternary alloy which has creep resistance up to 425 °C (an homologous temperature of 0.75) due to the slow-coarsening rate of the $Al_3(Sc_{1-x}Ti_x)$ precipitates.

Acknowledgements

This research is supported by the US Department of Energy through grant DE-FG02-98ER45721. Atom-probe tomographic measurements were performed at the Northwestern University Center for Atom-Probe Tomography (NUCAPT). The LEAP™ tomograph was purchased with funding from the NSF-MRI (DMR 0420532, Dr. Charles Bouldin, grant officer) and ONR-DURIP (N00014-0400798, Dr. Julie Christodoulou, grant officer) programs. Additionally, the LEAP tomograph was enhanced in April 2006 with a picosecond laser with funding from the ONR-DURIP (N00014-0610539, J. Christodoulou, grant officer). We thank Research Assistant Professor Dieter Isheim for managing NUCAPT. We also thank Keith Knipling and Richard Karnesky for interesting discussions.

References

[1] Knipling KE, Dunand DC, Seidman DN. Z Metallkd 2006;97(3):246–65.
[2] Hyland RW. Metall Trans A 1992;23A:1947–55.
[3] Jo HH, Fujikawa SI. Mater Sci Eng A 1993;171:151–61.
[4] Nakayama M, Furuta A, Miura Y. Mater Trans JIM 1997;38(10):852–7.
[5] Novotny GM, Ardell AJ. Mater Sci Eng A 2001;A318:144–54.
[6] Marquis EA, Seidman DN. Acta Mater 2001;49:1909–19.
[7] Iwamura S, Miura Y. Acta Mater 2004;52:591–600.
[8] Royset J, Ryum N. Mater Sci Eng A 2005;396:409–22.
[9] Fuller CB, Seidman DN, Dunand DC. Scripta Mater 1999;40:691–6.
[10] Marquis EA, Seidman DN, Dunand DC. Acta Mater 2002;50:4021–35.
[11] Harada Y, Dunand DC. Mater Sci Eng A 2002;329–331:686–95.
[12] Bergner D, Chi NV. Wissenschaftliche Zeitschrift der Padagogischen Hochschule "N.K. Krupskaja". Halle XV, Heft 3; 1977.
[13] Fujikawa SI. Defect Diffus Forum 1997;143–147:115–20.
[14] Van Dalen ME, Dunand DC, Seidman DN. Acta Mater 2005;53:4225–35.
[15] Fuller CB, Seidman DN. Acta Mater 2005;53:5415–28.
[16] Yoon KE, Noebe RD, Seidman DN. Acta Mater 2007;55:1159–69.
[17] Schmidt U, Beresina AL, Chuistov KV, Monastyrskaja TA, Rud AD. In: Ciach R, editor. Advanced light alloys and composites. Dordrecht: Kluwer Academic Publishers; 1998.
[18] Kuehmann CJ, Voorhees PW. Metall Mater Trans A 1996;27A:937–43.
[19] Fuller CB. Ph.D. thesis, Northwestern University; 2003.
[20] Toropova LS, Eskin DG, Kharakterova ML, Dobatkina TV. Advance aluminum alloys containing scandium. Gordon & Breach; 1998.
[21] Forbord B, Lefebvre W, Danoix F, Hallem H, Marthinsen K. Scripta Mater 2004;51:333–7.
[22] Tolley A, Radmilovic V, Dahmen U. Scripta Mater 2005;52:621–5.
[23] Fuller CB, Murray JL, Seidman DN. Acta Mater 2005;53:5401–13.
[24] Clouet E, Lae L, Epicier T, Lefebvre W, Nastar M, Deschamps A. Nat Mater 2006;5:482–8.
[25] Hallem H, Lefebvre W, Forbord B, Danoix F, Merthinsen K. Mater Sci Eng A 2006;421(1–2):154–60.
[26] Clouet E, Nastar M, Barbu A, Sigli C, Martin G. Solid–solid phase transformations in inorganic materials. TMS; 2005. p. 1–21.
[27] Murray JL, Peruzzi A, Abriata JP. J Phase Equilb 1992;13(3):277–91.
[28] Marquis EA, Seidman DN, Asta M, Woodward C, Ozolins V. Phys Rev Lett 2003;91:36101-1–3.
[29] Marquis EA, Seidman DN, Dunand DC. Acta Mater 2003;51:4751–60.
[30] Fuller CB, Seidman DN, Dunand DC. Acta Mater 2003;51:4803–14.
[31] Karnesky RA, Van Dalen ME, Dunand DC, Seidman DN. Scripta Mater 2006;55:437–40.
[32] Van Dalen ME, Dunand DC, Seidman DN. J Mater Sci 2006;41:7814–23.
[33] Karnesky RA, Seidman DN, Dunand DC. Mater Sci Forum 2006;519-521:1035–40.
[34] Kelly TF, Gribb TT, Olson JD, Martens RL, Shepard JD, Wiener SA, et al. Microsc Microanal 2004;10:373–83.
[35] Seidman DN. Annu Rev Mater Res 2007;37:127–58.
[36] Hellman OC, Vandenbroucke JA, Rüsing J, Isheim D, Seidman DN. Microsc Microanal 2000;6:437–44.
[37] Hellman OC, Vandenbroucke J, Blatz du Rivage J, Seidman DN. Mater Sci Eng A 2002;327(1):29–33.
[38] Hellman OC, Seidman DN. Mater Sci Eng A 2002;327(1):24–8.
[39] Tabor D. Br J Appl Phys 1956;7:159–65.
[40] Brown LM, Ham RK. In: Kelly A, Nicholson RB, editors. Strengthening methods in crystals. Amsterdam: Elsevier; 1971.
[41] Martin PW. Precipitation hardening. Oxford: Butterworth–Heinemann; 1998. p. 81.
[42] Frost HJ, Ashby MF. Deformation-mechanism maps: the plasticity and creep of metals and ceramics. Oxford: Pergamon; 1982.
[43] Ardell AJ. Metall Trans A 1985;16A:2131.
[44] Murken J, Girard O, Hohner R, Skrotzki B, Eggeler G. Mater Sci Forum 2000;331–337:1507–12.
[45] Nakajima T, Takeda M, Endo T. Mater Trans 2006;47(4):1098–104.
[46] Murray JL. Personal communication; 2003.
[47] Liu JZ, Ghosh G, van de Walle A, Asta M. Phys Rev B 2007;75:104117.
[48] Liu Z. Ph.D. thesis, Northwestern University; 2006.
[49] Peterson NL. J Nucl Mater 1978;69–70(1–2):3–37.
[50] Karnesky RA, Meng L, Dunand DC. Acta Mater 2007;55:1299–308.
[51] Marquis EA, Dunand DC. Scripta Mater 2002;47:503–8.
[52] Kaibyshev R, Sitdikov O, Mazurina I, Lesuer DR. Mater Sci Eng A 2002;A334:104–13.
[53] Morris MA. Philos Mag A 1992;65(4):943–60.
[54] Kaibyshev R, Musin F, Avtokratova E, Motohashi E. Mater Sci Eng A 2005;392:373–9.
[55] Cadek J, Kucharova K, Zhu SJ. Mater Sci Eng A 1999;272(45–56).

[56] Li Y, Nutt R, Mohamed FA. Acta Mater 1997;45(6):2607–20.
[57] Zhu SJ, Kucharova K, Cadek J. Met Mater Trans A 2000;31A:2229–37.
[58] Kucharova K, Zhu S, Cadek J. Kovove Mater 2002;40:69–84.
[59] Mohamed FA, Park K, Lavernia EJ. Mater Sci Eng A 1992;150:21–35.
[60] Mishra RS, Nandy TK, Greenwood GW. Philos Mag A 1994;69(6):1097–109.
[61] Takesue H, Oh-ishi K, Horita Z, Nemoto M. Mater Sci Eng A 1997;239–240:479–84.
[62] Lagneborg R. Scripta Metall 1973;7:605.
[63] Lagneborg R, Bergman B. Metal Sci 1976;10:20–8.
[64] Hausselt JH, Nix WD. Acta Metall 1977;25:1491.
[65] Rosler J, Arzt E. Acta Metall 1988;36(4):1043–51.
[66] Xiang Y, Srolovitz DJ. Philos Mag 2006;86(25–26):3937–57.
[67] Harada Y, Dunand DC. Scripta Mater 2003;48:219–22.
[68] van Dalen ME. Ph.D. thesis, Northwestern University; 2007.
[69] Knipling KE. Ph.D. thesis, Northwestern University; 2006.
[70] Knipling KE, Dunand DC. Scripta Mater 2008;59:387–90.
[71] Knipling KE, Dunand DC, Seidman DN. Acta Mater 2008;56(1):114–27.